Anisotropy of the structure factor of magnetic fluids under a field probed by small-angle neutron scattering

F. Gazeau,[1] E. Dubois,[2] J.-C. Bacri,[1,*] F. Boué,[3] A. Cebers,[4] and R. Perzynski[1,†]
[1]*Laboratoire des Milieux Désordonnés et Hétérogènes, UPMC Case 78, 4, Place Jussieu, 75252 Paris Cedex 05, France*
[2]*Laboratoire des Liquides Ioniques et Interfaces Chargées, UPMC Case 63, 4, Place Jussieu, 75252 Paris Cedex 05, France*
[3]*Laboratoire Léon Brillouin, CEA CNRS UMR 12, CE Saclay, 91191 Gif-sur-Yvette, France*
[4]*Latvian Academy of Sciences, Institute of Physics, LV-2169, Salaspils, Republic of Latvia*
(Received 10 July 2001; published 15 February 2002)

Small-angle neutron scattering is used to measure the two-dimensional diffraction pattern of a monophasic magnetic colloid, under an applied magnetic field. This dipolar system presents in zero field a fluidlike structure. It is well characterized by an interaction parameter K_T^0 proportional to the second virial coefficient, which is here positive, expressing a repulsion of characteristic length κ_0^{-1}. Under the field a strong anisotropy is observed at the lowest q vectors. The length κ_0^{-1} remains isotropic, but the interaction parameter K_T becomes anisotropic due to the long-range dipolar interaction. However, the system remains stable, the interaction being repulsive in all directions. Thus *we do not observe any chaining* of the nanoparticles under magnetic field. On the contrary, the revealed structure of our anisotropic colloid is a *lowering of the concentration fluctuations along the field* while the *fluidlike structure*, observed without field, is roughly preserved *perpendicularly to the field*. It expresses a strong anisotropy of the Brownian motion of the nanoparticles in the solution under applied field.

DOI: 10.1103/PhysRevE.65.031403 PACS number(s): 82.70.−y, 75.50.Mm, 28.20.Cz

I. INTRODUCTION

Magnetic fluids (MF) or ferrofluids (FF) [1–3] are colloidal suspensions in a liquid carrier of nanoparticles bearing a giant magnetic moment $\vec{\mu}$ of the order of 10^4 Bohr magnetons. Under an applied magnetic field $\vec{H}$, thanks to the interaction between $\vec{H}$ and the moment $\vec{\mu}$ of each particle and because of the dipolar magnetic interaction between particles, a ferrofluid becomes an anisotropic magnetic medium. The present paper addresses the question of the structure of such a ferrofluid at rest under a constant magnetic field.

From the theoretical point of view, the structure of dipolar systems, both without and with magnetic field, has been widely treated in literature. The pioneering paper by de Gennes and Pincus [4], written 30 years ago, proposed a chaining of magnetic particles due to the dipolar magnetic interaction. Later on, such a chaining was seen in numerical simulations [5–10] and considered theoretically [11]. This chaining has been observed experimentally in fluids involving an additional larger mesoscopic scale of the order of the micron: in emulsions of oily FF droplets in water or in dispersions of nonmagnetic colloids in FF [12–18]. Such a chaining, associated with a large distribution of characteristic times, has been suggested by magneto-rheological measurements on pure FF [19,20].

Contrary to the modelization of magneto-rheological fluids, a modelization accounting for the nanoparticles and their interactions appears at once highly complicated by two characteristics. First there is the strong influence of kT, and second the existence, in addition to dipolar interactions, of two isotropic interactions, that are the repulsion necessary for the stabilization of the solution and the van der Waals attraction. Several recent numerical simulations that take into account isotropic interactions show that the structure depends on the relative weight of isotropic and anisotropic contributions [8,9]. A dominating anisotropic dipolar interaction would lead to a chain formation as suggested by de Gennes and Pincus, whereas a dominating isotropic attraction would lead to gas-liquid-like phase separations as observed in [21–23]. A large community is interested in the nature of such phase transitions in MF [3,11,24–27].

From the experimental point of view, several points have to be mentioned. Firstly, an applied magnetic field can induce a separation of the sample in two phases. The fact that the observed system is really stable under field is often ambiguous, or not clearly established, in scattering experiments [28–33]. The risk is to study a phase-separated system of droplets, not a colloidal suspension. Secondly, an applied field can induce an anisotropy of the system at different levels: an anisotropy of the structure, of the dynamical behavior, and of the orientation of the magnetic moments. This last (magnetic) anisotropy can be studied using small-angle neutron scattering (SANS). SANS gives both a nuclear and a magnetic scattered intensity [34,35], the proportion of which depends on the experimental conditions. Thus, for a ferrofluid under field, an anisotropic scattering pattern can be observed even with a quasi-isotropic structure [35]. We are here not interested in this magnetic contribution, which will be analyzed in details in a forthcoming paper [36].

Experimentally, the fact that the structure factor of a magnetic colloid under field can be anisotropic was demonstrated 20 years ago in pioneering static works by small-angle x-ray scattering (SAXS) [28,29], and also recently [32]. However,

*Also at UFR de Physique Paris 7, 2, Place Jussieu, 75252 Paris cedex 05, France.
†Corresponding author. FAX: +33-1-44-27-38-54. Email address: rperz@ccr.jussieu.fr

 ©2002 The American Physical Society

no theoretical or definitive physical explanation of this anisotropy has been given until now. On the contrary, from a *dynamical point of view*, the anisotropy of the Brownian diffusion in a magnetic fluid under field, demonstrated experimentally at short scales by QEXS [32] and at larger scales in a forced Rayleigh scattering experiment [37,38], is theoretically modelized in [37,38].

In the present paper we aim to attain the clearest situation for a study of the structure of ferrofluids under a static magnetic field using SANS. The colloidal stability of the samples is clearly established (Sec. II). The magnetic contribution to the scattering is negligible: our data correspond to the nuclear scattering only and thus to the correlations of the particles spatial positions. After an analysis of the zero field results (Sec. III), we present our experiment under field and modelize this situation along the lines of thought of Refs. [37,38]. This allows us to correlate the SANS anisotropic pattern, associated with the fluctuations of concentration in the magnetic colloid, with the anisotropy of the long-range dipole-dipole interactions between particles.

II. FERROFLUID SAMPLES

A. Characteristics of the ionic ferrofluids

The ferrofluid solutions probed here are ionic ones. The nanoparticles are chemically synthesized in aqueous alkaline media according to Massart's method [39]. They are then, thanks to a coating of citrate ligands, dispersed either in water at $p\mathrm{H}=7$ or in glycerin. The nanoparticles are made of cobalt ferrite ($CoFe_2O_4$). They have a density $\rho=5\ \mathrm{g\,cm^{-3}}$ and their volume fraction Φ is determined by chemical titration of iron. As $CoFe_2O_4$ is ferromagnetic at room temperature, they bear a permanent magnetic moment $\vec{\mu}$. Its modulus is constant and equal to $\mu=m_s\pi d^3/6$, m_s being the magnetization of the nanoparticle material (taken equal to its bulk value $m_s=4\times10^5\ \mathrm{A\,m^{-1}}$) and d being the diameter of the ordered magnetic core of the particle, here of the order of 10 nm.

Let us comment that the diameter d of the magnetic core is slightly smaller (10% at most) than the physical diameter of the particle. There are two reasons for that—the layer of fluctuating disordered spins [40,41] present at the surface of the magnetically ordered core inside the nanocrystal and the layer of citrate species adsorbed on the nanocrystal. The thickness of each of these layers is a few angstroms.

The particles also bear a superficial negative density of charges Σ coming from the citrate ligands adsorbed at their surface. In such solutions the adsorbed species are always in equilibrium with free species. Thus Σ is a function of $[\mathrm{citrate}]_{free}$, the concentration of free citrates [see Fig. 1] for aqueous solutions at $p\mathrm{H}=7$ [22,42]. In the present aqueous samples, Σ is always at saturation, as we roughly fix $[\mathrm{citrate}]_{free}\approx0.5\Phi\ \mathrm{mol\,L^{-1}}$: Σ is always of the order of 1.7 electronic charges per $\mathrm{nm^2}$ as $[\mathrm{citrate}]_{free}$ varies from $\approx3.5\times10^{-3}\ \mathrm{mol\,l^{-1}}$ at $\Phi=0.7\%$ up to $\approx0.1\ \mathrm{mol\,l^{-1}}$ at Φ of the order of 20%. For the samples in glycerin the curve of Fig. 1 is qualitatively similar but shifted toward lower $[\mathrm{citrate}]_{free}$ concentrations. In our conditions the charge is also at saturation in glycerin.

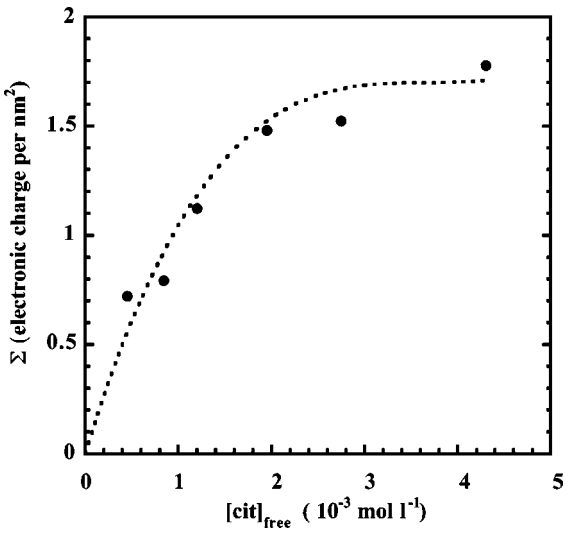

FIG. 1. Superficial density of electrostatic charge Σ of the nanoparticles dispersed in water at $p\mathrm{H}=7$ as a function of the free citrate concentration $[cit]_{\mathrm{free}}$.

B. Colloidal stability

An important requirement for understanding anisotropic interactions is that the studied sample remains a monophasic dispersion, even under an applied magnetic field (here up to $68\ \mathrm{kA\,m^{-1}}$). Detailed studies on the colloidal stability of chemically synthesized ionic ferrofluids [39] have been recently performed [23,42–44]. In particular, for γ-Fe_2O_3 nanoparticles, the interparticle interactions have been precisely quantified through a measurement of the second virial coefficient A_2 of the osmotic pressure π and correlated both to the chemical characteristics of the colloids and to their experimental colloidal phase diagram (π versus Φ) [21–23]. Although the material is slightly different, the studied cobalt ferrite nanoparticles are comparable to γ-Fe_2O_3 nanoparticles for the charge (i.e., the electrostatic repulsion), for the van der Waals attraction and for the dipolar interaction. The phase diagram in zero field (plotted in Fig. 2) is thus of the same kind: the samples are monophasic for high pressures and separate into a ''liquid'' plus a ''gas'' phases for pressures lower than the critical point.

The colloidal stability of our ionic ferrofluids has also been explored under an *external magnetic field* [42,43]. Three different situations may be encountered for an initially monophasic ionic FF.

(i) The interparticle repulsion is so strong that an applied field has no effect either on the colloidal stability or on the structure factor of the colloid [21,22]. This would correspond to very high osmotic pressures.

(ii) The interparticle repulsion is weak, making an applied field (in the same way as does a temperature decrease) able to induce a colloidal phase separation [39]. This leads then to elongated needles (of typical size 100 μm) of a concentrated liquid phase in coexistence with a dilute one—this behavior is observed with ionic FF but also with oily ones [45,46]. This would correspond to pressures close to the two-phases area, where $A_2<0$ in Fig. 2 (equivalently $K_T<0$; see below).

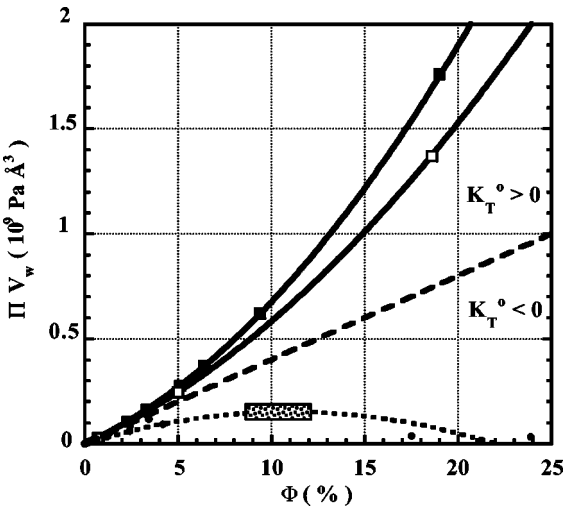

FIG. 2. Diagram πV_w versus volume fraction Φ. Full lines: equations of state of samples A (■) and B (□) as calculated from the present SANS results. Dashed line: equation of state of perfect gas ($K_T^0=0$). Dotted line: guide for the eye of the phase diagram (small dots) from Ref. [23] obtained for citrated ionic ferrofluids based on γ-Fe_2O_3 nanoparticles. Dotted rectangle: critical area as evidenced in [43,44].

(iii) An intermediate possibility, investigated in the present paper, is that the balance of the interparticle interactions is globally repulsive in zero field ($A_2>0$) and remains globally repulsive under the applied magnetic field. In practice, the colloidal dispersions studied here remain monophasic in our range of applied field and temperature, owing to their chemical characteristics. This point is checked by light scattering and optical microscopy observation.

C. Magnetic properties

The magnetic moment of the nanoparticles is of the order of 10^4 Bohr magnetons and can be here considered as blocked in the particle along the easy direction of magnetization [47]. Thanks to the rotational degrees of freedom of the nanoparticles in the liquid carrier, the resulting medium behaves, under an applied field $\vec{H}$, like a giant paramagnetic material [1].

In the *dilute regime* where the *interparticle interaction is negligible* [48] ($\Phi \leqslant 1\%$), the magnetization curve $M(H)$ can be described by a Langevin formalism

$$M = m_s \Phi L(\xi) \quad \text{with} \quad L(\xi) = \coth(\xi) - \xi^{-1}, \tag{1}$$

$L(\xi)$ being the Langevin function and $\xi = \mu_0(\mu H/kT)$ the Langevin argument with μ_0 the vacuum permeability, k the Boltzmann constant, and T the temperature; ξ is particle size dependent. Assuming a log-normal distribution of diameters $P(d) = (1/\sqrt{2\pi}\sigma d)\exp\{[\ln^2(d/d_0)/2\sigma^2]\}$, $M(H)$ measurements [48] can be adjusted to determine a mean magnetic size $d_0 = \exp(\langle \ln d \rangle)$ and a standard deviation σ. Table I gives d_0 and σ for the two present samples.

At finite concentration, in order to take into account the magnetic interparticle interaction under the applied field we use, in a mean field approximation, *an effective field model*, and the magnetization then writes [3]

$$M = \Phi m_s L(\xi_e) \tag{2}$$

with ξ_e given by the self-consistent equation

$$\xi_e = \xi + \lambda \gamma L(\xi_e), \tag{3}$$

where λ is the effective field constant and γ is the dipolar interaction parameter.

If the effective field constant λ is null, we recover expressions (1) without interparticle interactions. The classical Lorentz value [49] of λ is 0.33. In [37,38], a value $\lambda = 0.22$ has been found for ferrofluid solutions.

The dipolar interaction parameter γ writes $\gamma = \mu_0(\mu^2/r^3 kT)$ where r is the mean interparticle distance. This parameter γ is the ratio of the energy of dipolar interaction to the thermal energy kT, for two aligned dipoles. It can be rewritten as

$$\gamma = \mu_0 m_s^2 \frac{\pi d^3}{6} \frac{\Phi}{kT}. \tag{4}$$

Thus, *in the whole range of volume fractions*, γ is proportional to Φ. The quantity γ/Φ is a *constant* characteristic of the nanoparticles and *independent of* Φ which can be easily determined from *measurements at low volume fractions*. If $\Phi \ll 1$, then $\xi_e \approx \xi$ and γ is simply related to the initial magnetic susceptibility $\chi_0 = M/H$ through the Langevin expression (1): it writes $\gamma = 3\chi_0$ thus $\gamma/\Phi = 3\chi_0/\Phi$.

Table I gives the value of the constant $\gamma/\Phi = 3\chi_0/\Phi$ obtained for each sample from a χ_0 measurement at low Φ. In this work, Φ ranges between 1% and 19% (see Table I), thus the maximum value of γ is here $\cong 8$. These γ and γ/Φ values are compatible with the colloidal stability of the sample under field. To establish that, let us consider the mean field derivation [3] of the phase separation which defines, in the framework of a cgs unit system, a threshold value for the parameter μ^2/d^3kT ranging from 4.08 (zero field) to 3.375 (infinite field). Returning to SI this parameter becomes $\mu_0(\mu^2/d^3kT)$ with threshold values $4.08 \times 4\pi$ and $3.375 \times 4\pi$. This leads here (in SI) to $\gamma/\Phi = (6/\pi)\mu_0(\mu^2/d^3kT) = 98$ in zero field and 81 in infinite field. Our samples have significantly lower γ/Φ values (see Table I) which are a warrant for stability. Table II details the FF solutions studied under applied magnetic field, recalling in each situation the values of the parameters γ and ξ. In the present experiments under magnetic field, the magnetization is never fully saturated. In the largest field, M reaches at most 75% of its saturation value.

III. SANS IN ZERO MAGNETIC FIELD

A. Experimental conditions

The scattering experiments are performed in the Laboratoire Léon Brillouin (LLB) Saclay, on the PAXE and PAXY spectrometer of the LLB (CEA-CNRS) in the reactor Orphée (CE-Saclay, France). The neutron wavelength is $\lambda = 10$ Å the detector distance is 3.2 m, leading to a scattering vector q

TABLE I. Characteristics of the ferrofluid solutions. Δl^2 is the nuclear contrast of the nanoparticles with respect to the liquid carrier. Φ is the volume fraction of the nanoparticles obtained from a chemical titration of iron. The mean diameter d_0 and the standard deviation σ of the log-normal distribution are deduced from the magnetization measurements at low Φ (see text). The weight-averaged diameter d_w^{calc} and the gyration radius R_g^{calc} are calculated from the magnetic size characteristics d_0 and σ. The parameters d_w, R_g, K_T^0, and A_2 are deduced from SANS measurements in zero field [see Figs. 2(a) and 2(b)]. The dipolar interaction parameter γ/Φ is deduced experimentally from initial susceptibility measurements *at low* Φ.

Sample	A	B
Liquid carrier	water	glycerine
Δl^2 (cm^{-4})	4.53×10^{21}	3.12×10^{21}
d_0 (nm)	9.5	6.8
σ	0.3	0.4
d_w (nm)	14.0	15.3
d_w^{calc} (nm)	14.2	14
R_g (nm)	8.1	8.8
R_g^{calc} (nm)	8.9	10.4
K_T^0	13.8	9.1
A_2 ($\mathrm{mol\,cm^3\,g^{-2}}$)	3×10^{-7}	1.6×10^{-7}
γ/Φ	42 ± 1	39 ± 2
Φ	0.7%, 2.3%, 3.3% 5.1%, 6.4%, 9.4%, 19%	0.7%, 5%, 19%

ranging from 0.01 to 0.07 $\mathrm{Å}^{-1}$. The fluid dispersion is introduced between two quartz disks separated by an annular spacer, the thickness of which lies between 0.1 and 1 mm, depending on the volume fraction of particles. The intensity of the scattered neutrons is recorded on a plane as a function of the scattering vector $\vec{q}$. A data treatment is applied in order to subtract the scattering from the solvent and the quartz cell. In all the figures the error bars on the scattered intensity are smaller than the symbols.

TABLE II. Measurements under applied field—sample characteristics. The dipolar interaction parameter γ is deduced from Table I. The Langevin parameter ξ is evaluated with $\xi=\gamma H/m_s\Phi$ using $\gamma/\Phi=41$ and $m_s=4\times10^5$ $\mathrm{A\,m^{-1}}$.

Sample	Φ	γ	H ($\mathrm{kA\,m^{-1}}$)	ξ
A	0.7%	0.3	68	6.9
A	6.4%	$2.7\pm.1$	68	6.9
A	19%	$8.0\pm.2$	28.4	2.9
			40.8	4.2
			68	6.9
B	0.7%	0.2	27.2	2.8
B	5%	1.9 ± 0.1	9.6	1
			16.4	1.7
			27.2	2.8
B	19%	7.4 ± 0.4	8	0.8
			16.4	1.7
			27.2	2.8

As pointed out previously, the scattering of neutrons by a magnetic colloid may have two different origins: either nuclear interactions with all nuclei of the sample, or magnetic interaction between neutron spins and local fields. The magnetic cross section, proportional to μ^2 and to the number of particle per volume unit, can be evaluated from the magnetization M of our cobalt ferrite particles [50]. If the particles are dispersed in a hydrogenated solvent, the magnetic scattering is less than 2% of the total cross section. This point is experimentally confirmed by a polarization analysis performed with the spin-echo diffractometer of Laboratoire Léon Brillouin (CEA-CNRS) in the reactor Orphée (CE-Saclay, France) [36,42]. We therefore neglect magnetic scattering and are just left with scattering by nuclei.

The respective scattering length densities of $CoFe_2O_4$, water, and glycerin are 6.2×10^{10} cm^{-2}, 0.614×10^{10} cm^{-2}, and -0.53×10^{10} cm^{-2}. Table I gives the resulting contrast between the particles and the two solvents, which are equivalent in this respect. They mostly differ in their viscosity; however, from the static point of view of the present study, this has no effect.

B. Theoretical background

Although the scattering of a usual dispersion of particles is well known, we recall here the main formulas for a clear definition of coefficients before adding a new term, the contribution coming from the applied field. We start from the scattered intensity I (cm^{-1}) of a colloidal dispersion of spherical and solid magnetic particles in mutual interaction. It may be written in zero magnetic field as

$$I(q,\Phi)=\Delta l^2\Phi V_w F(q)S(q,\Phi). \tag{5}$$

where Δl^2 is the squared difference of scattering length densities (in cm^{-4}) between the nanoparticles and the solvent carrier, Φ the volume fraction of nanoparticles, V_w their weight average volume, $F(q)$ the particle form factor, and $S(q,\Phi)$ the structure factor of the solution. Here the scattering is isotropic. The intensity, the form factor, and the structure factor depend on the scattering vector only through its *modulus*: $q=|\vec{q}|$.

The *form factor* of isolated spherical particles can be written in the low q limit as

$$F(q)\approx\exp\left(-\frac{1}{3}q^2R_g^2\right) \quad \text{if } qR_g\leqslant1, \tag{6}$$

where R_g is the radius of gyration of the nanoparticles.

The *structure factor* $S(q,\Phi)$ expresses the structure of the colloid, that is the spatial distribution of the centers of mass of the nanoparticles under their mutual interactions. In the high q limit, it is independent of q and Φ and it is equal to 1. In the small but finite q limit, the structure factor can be expanded in q^2, as we will see now.

Let us develop the free energy density f of the solution as a Ginzburg-Landau expansion [51] in Φ and $\nabla\Phi$. The variation of f, up to the second order term in concentration fluctuations, can be written as

$$\frac{1}{2}\delta^2 f = \frac{1}{2\Phi}\frac{\partial \pi}{\partial \Phi}(\delta\Phi)^2 + \frac{b_0}{2}(\nabla(\delta\Phi))^2, \tag{7}$$

where π is the osmotic pressure of the solution. This energy functional describes the concentration fluctuations in the continuum limit. The second term is the energy cost associated with their spatial inhomogeneities. Expressing the free energy through Fourier components $\delta\Phi_{\vec{q}} = (1/\sqrt{V})\int \delta\Phi \exp(i\vec{q}\cdot\vec{r})dV$ of the concentration fluctuations, the structure factor of the solution at small q can be written as

$$S(q,\Phi)^{-1} = \frac{\Phi V_w}{\langle |\delta\Phi_{\vec{q}}|^2 \rangle} = \frac{V_w}{kT}\left(\frac{\partial \pi}{\partial \Phi} + b_0 q^2 \Phi\right). \tag{8}$$

We see from Eq. (8) that in the limit $q \to 0$, $S(q,\Phi)$ is proportional to the osmotic compressibility of the solution. $\partial\pi/\partial\Phi$ is usually written at low Φ as a virial development,

$$\frac{\partial \pi}{\partial \Phi} \cong kT\left(\frac{1}{V_w} + 2\rho^2 A_2 N_a \Phi\right), \tag{9}$$

ρ being the particle density, A_2 the second virial coefficient of the osmotic pressure, and N_A the Avogadro number. Combining Eqs. (8) and (9) we obtain

$$S(q,\Phi)^{-1} \cong 1 + K_T^0 \Phi (1 - q^2 \kappa_0^{-2}) \tag{10}$$

where

$$K_T^0 = 2\rho^2 A_2 V_w N_a \quad \text{and} \quad -K_T^0 \kappa_0^{-2} = \frac{b_0 V_w}{kT}$$

κ_0^{-1} being a characteristic length. Here the interparticle potential is repulsive, K_T^0 is positive, and b_0 is negative. In this situation, at $q \to 0$, there is no correlation domain associated to the fluctuations of concentration, see Appendix A (the opposite case would correspond to large scales fluctuations for a system close to a phase separation [52]). The fluctuations of position of the particles are here individual fluctuations associated with a correlation hole of order κ_0^{-1}.

Let us now focus on the signification of this length κ_0^{-1}. For that purpose, we introduce the direct correlation function $C(q) = (V_w/\Phi)[1 - S^{-1}(q,\Phi)]$. $C(q)$ is the Fourier transform of $C(r)$, which is related to the interparticle potential $V(r)$: as a first approximation, $C(r) = -V(r)/kT$ [53]. If $V(r) \approx \exp(-\kappa_0 r)/r$ with a potential range κ_0^{-1}, then $C(q) = -V_w K_T^0 (1 - q^2 \kappa_0^{-2})$. However, the potential between the cobalt ferrite nanoparticles is more complicated for different reasons: the scattering objects are not points, they have a spatial extension and the finite size of the particles cannot be neglected. The potential is a combination of hard sphere repulsion (HS), van der Waals attraction (VdW), electrostatic repulsion (elec), and dipolar interaction (dip).

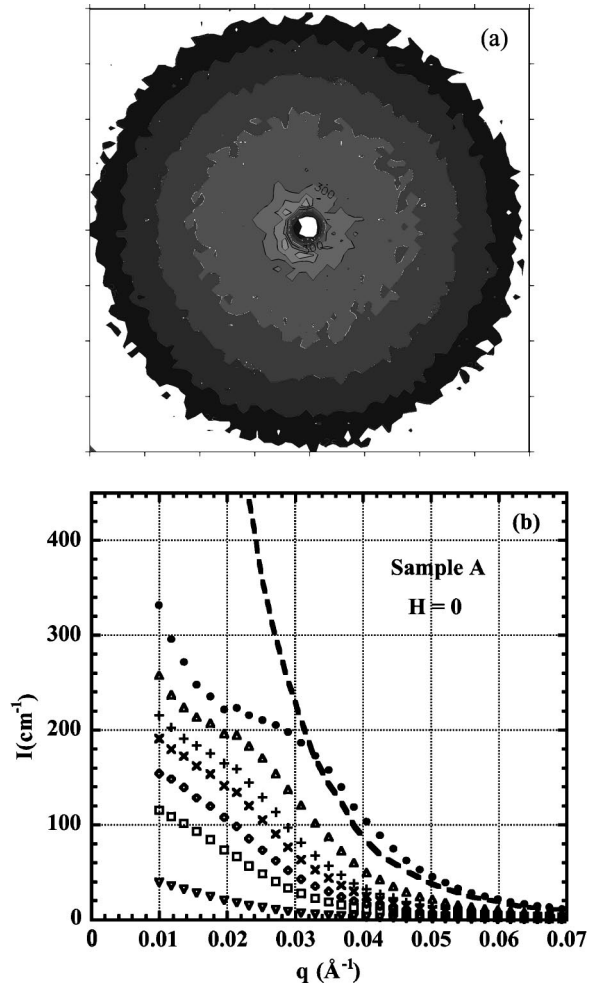

FIG. 3. Sample A in zero applied field. (a) Isotropic 2D scattering pattern at $\Phi = 19\%$. The contour lines are isointensity profiles. (b) Intensity I averaged on rings at constant scattering vector q as a function of q at various volume fractions [from top to bottom $\Phi = 19\%$ (●); 9.4% (△); 6.4% (+); 5.1% (×); 3.3% (◇); 2.3% (□); and 0.7% (▽)]. The dashed line corresponds to the computed intensity $F^*(q, \Phi = 19\%)$.

Thus we can write $\kappa_0^{-2} = \Sigma_i A_i \kappa_i^{-2}$, where the A_i are coefficients, respectively, depending on the characteristics of interaction i (i = HS, VdW, el, or dip). In all cases, κ_0^{-1} is characteristic of the range of the interactions between particles; however, simple limits only can be written easily. First, if the salt concentration is low, $\kappa_{\text{elec}}^{-1}$ dominates. Because of the finite size of the particles, $\kappa_{\text{elec}}^{-1}$ is not exactly the Debye length but depends on it. Second, if the salt concentration is high, A_{elec} is negligible. If A_{VdW} and A_{dip} are negligible compared to A_{HS} then κ_0^{-1} reduces to $\kappa_{\text{HS}}^{-1} = D/\sqrt{10}$ (D being the hard sphere diameter), at the level of the second virial approximation.

C. Results

Whatever the sample and the volume fraction of the solution, the neutron scattering in zero field is isotropic [see Fig. 3(a)]. The intensity $I(q,\Phi)$ obtained for sample A after av-

eraging on a ring at constant q is given in Fig. 3(b). The scattered intensity is at low Φ a monotonously decreasing function of q and presents at the largest Φ a small bump at an intermediate scattering vector q. Whatever q, the intensity is an increasing function of Φ.

A closer look at low q shows, while q decreases, an increase of intensity for the largest sample concentrations: this could be possibly explained by an agglomeration of the nanoparticles as Φ increases. In order to check that we are not concerned by such a process, let us take the case of $\Phi = 19\%$ and compare in Fig. 3(b) the intensity $I(q,\Phi = 19\%)$ to the quantity $F^*(q,\Phi) = \Phi[\Delta l^2 V_w F(q)]$ [taken at $\Phi = 19\%$ and where $F(q)$, the *form factor* of the particles is deduced from the low Φ measurements by an extrapolation at $\Phi = 0$ of the ratio $I(q,\Phi)/\Phi$]. $F^*(q,\Phi)$ would be the scattered intensity in the absence of interparticle interactions. In Fig. 3(b), $F^*(q,\Phi = 19\%)$ is for $q < 3\times 10^{-2}$ Å^{-1} clearly larger than $I(q,\Phi = 19\%)$. This inequality is true for all the other Φ values. It is the proof that the increase of intensity observed at low q for the largest sample concentrations cannot be explained by an agglomeration of the nanoparticles as Φ increases. This process would indeed have induced an increase of the volume V_W of the scattering entities and thus a scattered intensity larger than $F^*(q,\Phi)$. On the contrary the difference between $F^*(q,\Phi = 19\%)$ and $I(q,\Phi = 19\%)$ has to be addressed to a structure factor smaller than 1 at low q and large Φ [see expression (5)]. The upturn for $q \to 0$ (at large Φ) of $I \propto \Phi F(q) S(q,\Phi)$ is the result of the product of a function continuously decreasing with q, $\Phi F(q)$, by a nonmonotonous function of q, $S(q,\Phi)$, which remains constant.

1. Particle size characteristics and interaction parameter K_T^0

This section is based upon expressions (5) and (10). As said above $\Delta l^2 V_w F(q)$ is deduced from a linear extrapolation at $\Phi = 0$ of the ratio $I(q,\Phi)/\Phi$. As shown in Fig. 4(a) for sample *A*, a semilogarithmic plot of $\Delta l^2 V_w F(q)$ versus q^2 provides via a linear fit to expression (6) the radius of gyration R_g; radii for samples *A* and *B* are given in Table I.

We also extract $\Delta l^2 V_w$ and K_T^0 from the data at $q \to 0$ using expression (10). A linear adjustment of $[\Phi/I(q,\Phi)]_{q=q_{\min}}$ as a function of Φ, is made for $q_{\min} = 10^{-2}$ Å^{-1} [see Figure 4(b)]. Here $[\Phi/I(q,\Phi)]_{q=q_{\min}}$ is assimilated to $\lim_{q\to 0}[\Phi/I(q,\Phi)] = (1/\Delta l^2 V_w) S^{-1}(q=0,\Phi)$, as for $q \to 0$ $F(q)$ reduces to 1. Knowing Δl^2, we can then compare for the two samples, the two particle sizes R_g, and $d_w = (6V_w/\pi)^{1/3}$ determined by neutron scattering to the ones expected from the magnetic size distribution [48,54] (Table I). They are in reasonable agreement.

The coefficient K_T^0 is indeed found here positive and of the order of 10 for both samples. It expresses that, on average, the total interparticle interaction is repulsive. The second virial coefficient of the osmotic pressure, A_2, which is proportional to K_T^0, is also positive and here of the order of a few 10^{-7} cm^3 g^{-1} mol. Knowing A_2, we calculate the osmotic pressure π of each of our FF solutions and can locate those samples on the phase diagram of Fig. 2 described in Sec. II B.

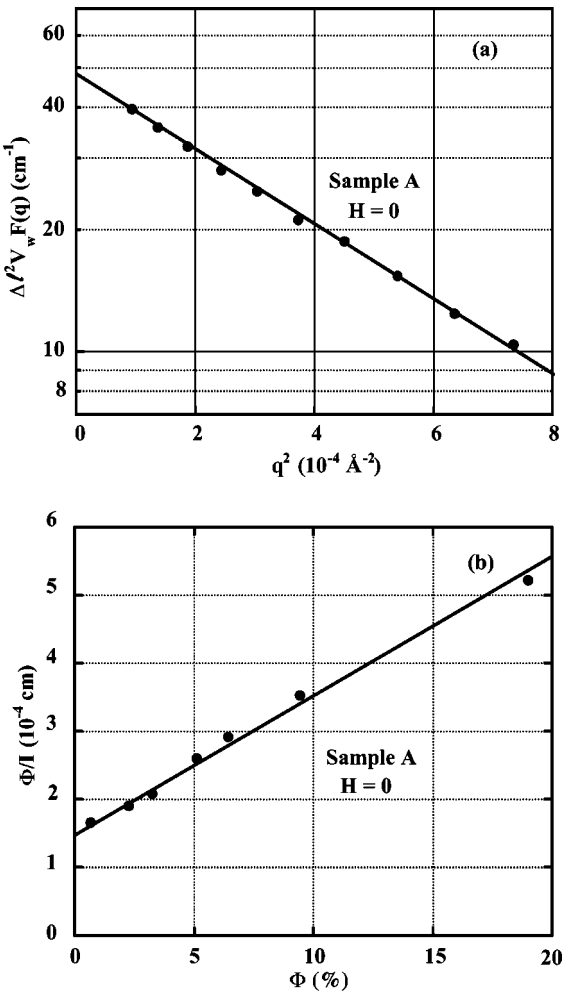

FIG. 4. Sample A in zero applied field. (a) Guinier plot of $\Delta l^2 V_w F(q)$ as a function of q^2. The full line corresponds to $R_g = 81$ Å. (b) Plot of Φ/I at $q = q_{\min} = 7\times 10^{-3}$ Å^{-1} as a function of Φ. The full line corresponds to $K_T^0 = 13.8$.

2. Structure factor and characteristic correlation length κ_0^{-1}

The structure factor $S(q,\Phi)$ of the FF solutions is deduced from $I(q,\Phi)$, knowing $F(q)$. We show it in Fig. 5 for sample *A* at various Φ. For the largest volume fraction $\Phi = 19\%$, the structure factor exhibits a distinctive maximum at a scattering vector $q_{\text{bump}} = 4.3\times 10^{-2}$ Å^{-1}. This corresponds to a distance $D_{\text{bump}} = 2\pi/q_{\text{bump}} \cong 145$ Å very close to the mean interparticle distance $d(\pi/6\Phi)^{1/3}$ (= 145 Å) deduced from the volume fraction of the solution.

From $S(q,\Phi)$, we can also, at $q \to 0$, determine the coefficient b_0 of the fluctuation term in the free energy development (7) [or equivalently the characteristic length κ_0^{-1} of Eq. (10)]. The quantity $(1/\Phi)[S(q,\Phi)^{-1} - 1] = -C(q)/V_w$ can be plotted as a function of q^2; as shown in Fig. 6(a) for sample A at $\Phi = 5.1\%$. At low q, $-C(q)/V_w$ decreases linearly as a function of q^2, starting from the value K_T^0 at $q = 0$, and with a slope equal to $b_0 V_w/kT = -K_T^0 \kappa_0^{-2}$ [see expression (10)]. From Fig. 6(a) we obtain for sample A at $\Phi = 5.1\%$: $K_T^0 = 14$, $b_0 V_w/kT = -3.2\times 10^4$ Å^2, leading to $\kappa_0^{-1} = 48$ Å and $b_0/kT = -2.2\times 10^{-2}$ Å^{-1}.

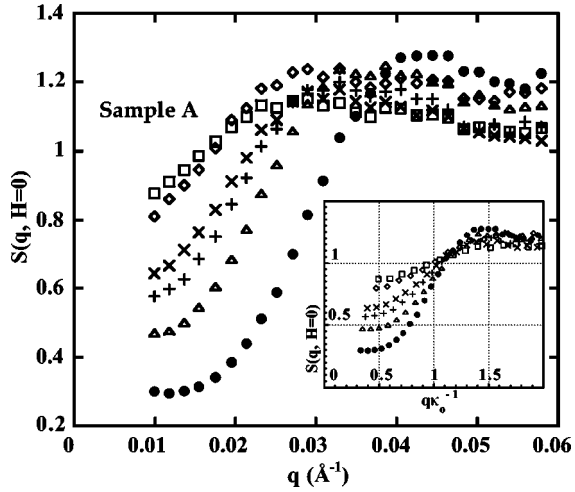

FIG. 5. Structure factor $S(q,H=0)$ versus the scattering vector q for sample A at $H=0$ for various volume fractions Φ [same symbols as in Fig. 3(b)]. Inset: $S(q,H=0)$ as a function of the reduced parameter $q\kappa_o^{-1}$.

This length κ_0^{-1} allows us to rescale the structure factors $S(q,\Phi)$: plotted versus $q\kappa_0^{-1}$, the different curves all snip together and the intersection point corresponds to $q\kappa_0^{-1}\sim 1$ and $S(q,\Phi)\sim 1$ [see the inset of Fig. 5(a)]. Moreover, the plot of $-C(q,\Phi)/K_T^0 V_w$ versus $q^2\kappa_0^{-2}$ leads whatever Φ to a linear master curve in the range $0<q\kappa_0^{-1}<1$ [see Fig. 6(b)]. These two representations express that the development of expression (10) is valid up to $q=\kappa_0$, i.e., for q larger than expected, and validates the experimental determination of κ_0^{-1}.

Whatever the sample and the volume fraction, b_0 is here negative, $K_T^0>0$, and κ_0^{-1} is defined. The range κ_0^{-1} of the interparticle potential is plotted in Fig. 7 as a function Φ: it is a decreasing function of Φ. The samples are prepared by diluting the most concentrated one with pure water; the ionic strength in our samples is proportional to Φ.

For the highest Φ the ionic strength is high ($[\text{citrate}]_{\text{free}} \approx 0.1\ \text{mol l}^{-1}$), the electrostatic repulsion is screened, and this sample may exhibit a behavior close to that of a hard sphere system (see Sec. III B). It is indeed what we observe. Let us consider a hard sphere diameter of 100 Å, we obtain $\kappa_{\text{HS}}^{-1}\sim 32$ Å. It is close to the experimental value of κ_0^{-1} obtained at $\Phi=19\%$.

For lower Φ, the lower ionic strength makes the range of the repulsion larger and contributes to increase κ_0^{-1}, which becomes larger than for hard spheres. Note that extra experiments, not presented here and performed at constant ionic strength with other samples, lead to a value for κ_0^{-1} that is independent of Φ.

IV. SANS UNDER APPLIED MAGNETIC FIELD

A. Experimental scattered intensity: overview of its anisotropic character

Using the same spectrometer configuration as described above in Sec. III, the experiment is now performed under a magnetic field $\vec{H}=H\vec{h}$, $\vec{h}$ being the unit vector along the field direction. It is applied in the plane of the sample cell (i.e., perpendicular to the neutron flux) and ranges between 0 and 680 kA/m (see the summary in Table II).

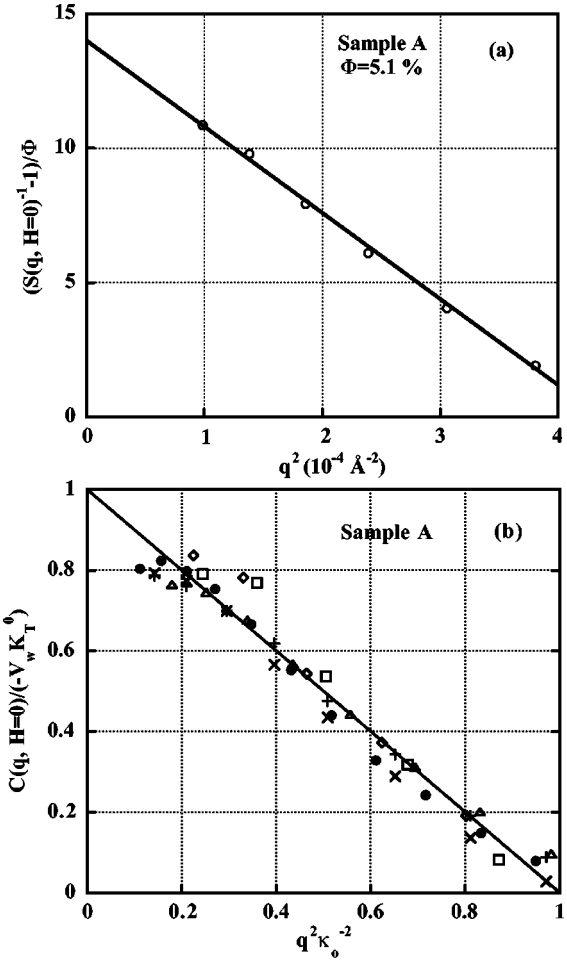

FIG. 6. Sample A at $H=0$. (a) Plot of $[S(q,H=0)^{-1}-1]/\Phi$ as a function of q^2 at $\Phi=5.1\%$ and $q<2.2\times10^{-2}$ Å^{-1}. The full line is the best fit of the data by Eq. (10) with $K_T^0=13.8$ and $\kappa_0^{-1}=48$ Å. It corresponds here to $b_0V_w/kT=-3.2\times10^4$ Å^2. (b) Direct correlation function in a reduced representation $C(q,H=0)/-V_wK_T^0=[S(q,H=0)^{-1}-1]/K_T^0\Phi$ as a function of $q^2\kappa_0^{-2}$. Same symbols as in Fig. 3(b). The full line corresponds to Eq. (10).

Under applied field, the scattering becomes anisotropic, as can be seen by various representations of the intensity.

(i) 2D patterns [Fig. 8(a)] of equal intensity contours.

(ii) By plotting the counting along a ring as a function of the angle $\theta=(\vec{q},\vec{h})$ between the scattering vector and the field [Fig. 8(b)]. The anisotropy of the pattern is strong at low q (along a circle of radius at $q=0.02$ Å^{-1} the intensity varies sinusoidally with θ; such that $I_{\max}/I_{\min}\approx 2$) and smooths out progressively as q increases (along a circle at $q=0.06$ Å^{-1}, the intensity does not vary with θ, thus is basically isotropic).

(iii) By radial averaging of the intensity in sectors of $\pm 15°$ along the directions perpendicular to the field ($\vec{q}\perp\vec{h}$) and parallel to it ($\vec{q}\parallel\vec{h}$), leading respectively to $I_\perp(q)$ and $I_\parallel(q)$ as shown in Fig. 9. If we compare with the radially

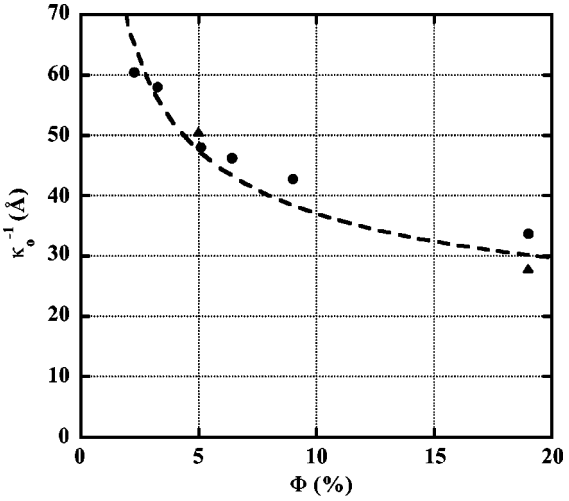

FIG. 7. Plot of κ_0^{-1} as a function of Φ for samples A (●) and B (▲). The dashed line is a guide for the eye.

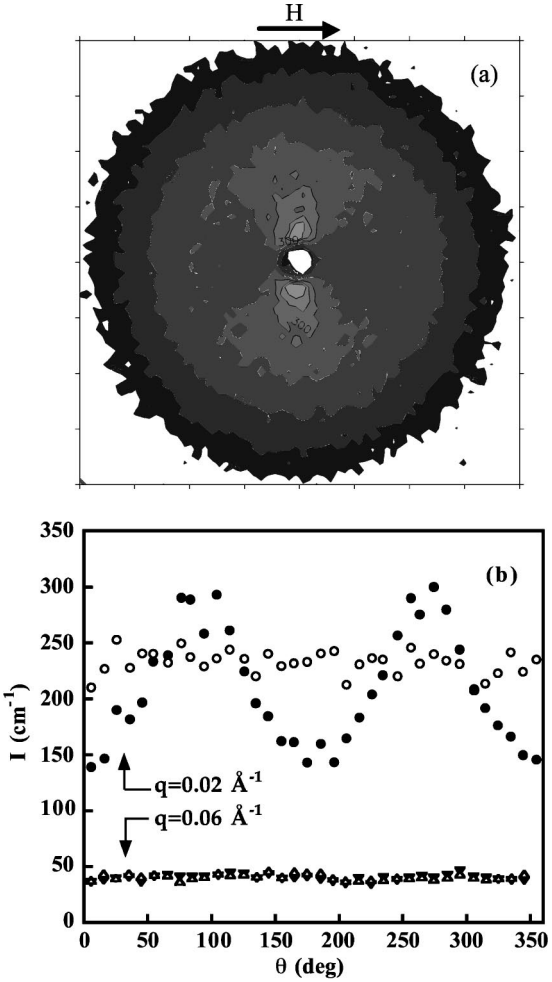

FIG. 8. Sample A at $\Phi=19\%$. (a) Anisotropic 2D scattering pattern under a horizontal field $H=68$ kA m^{-1}. (b) Angular dependence of the scattered intensity I at two different scattering vectors ($q=2\times10^{-2}$ Å^{-1} and 6×10^{-2} Å^{-1}) in zero field (open symbols) and under $H=68$ kA m^{-1} (full symbols).

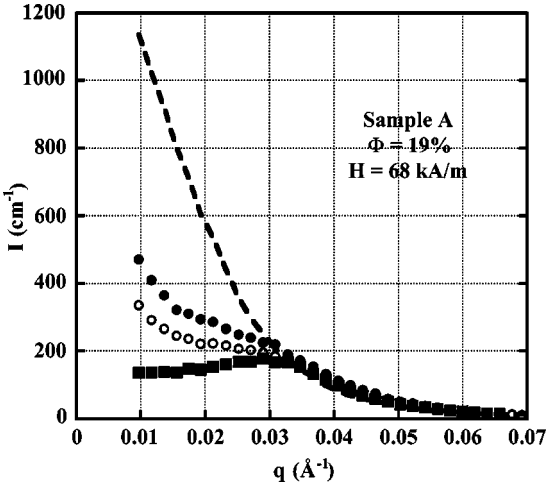

FIG. 9. Sample A at $\Phi=19\%$. A comparison among the scattered intensity $I(q)$ at $H=0$ averaged on rings at constant q (open symbols); the anisotropic intensities at $H=68$ kA m^{-1} averaged on a sector of $\pm15°$ along the field direction ($I_\parallel$ for $\theta=0$: ■) and perpendicular to the field direction ($I_\perp$ for $\theta=\pi/2$: ●); and the quantity $F^*(q,\Phi=19\%)$ determined in zero field (dashed line).

averaged intensity $I_{H=0}(q)$ at $H=0$, we note the following: (i) At low q, compared to $I_{H=0}(q)$, $I_\perp(q)$ shows an excess of scattering, while $I_\parallel(q)$ shows a deficiency. (ii) For progressively increasing q, the order $I_\perp(q)\geqslant I_{H=0}(q)>I_\parallel(q)$ is kept; however, this hierarchy progressively vanishes until the largest q are reached, then $I_\perp(q)\cong I_{H=0}(q)\cong I_\parallel(q)$.

In the same way that we have checked for the absence of particle agglomeration without applied magnetic field, we can check it now under field. Since $I_\perp(q)$ never reaches $F^*(q,\Phi=19\%)$, the intensity expected for noninteracting particles (see Fig. 9; curve for F^* is a dotted line), agglomeration is absent. In other words, an applied field does not affect V_w and $F(q)$, therefore, does not produce a phase separation.

Let us also note that $I_\parallel(q)$ and $I_\perp(q)$ are not proportional: $I_\perp(q)$ is monotonically decreasing with q while $I_\parallel(q)$ is not monotonic. The anisotropy of $I(\vec{q})$ under field has then to be related to an anisotropy of the structure factor which has to be written as $S(\vec{q},\Phi)$ or $S(q,\theta,\Phi)$.

B. Analysis of the experimental structure factor

1. Direct observation

Assuming thus that the form factor $F(q)$ is the same as in zero field, we deduce from the average of the scattered intensity on $\pm15°$ sectors (see Fig. 9) $S_\parallel(q,\Phi)$ at $\theta=0$ and $S_\perp(q,\Phi)$ at $\theta=\pi/2$. They are plotted on Fig. 10 for sample A at $\Phi=19\%$ and $H=68$ kA m^{-1}. They are compared to the isotropic structure factor $S_{H=0}(q,\Phi=19\%)$ obtained previously at $H=0$. We observe the following.

(i) The maximum of $S_{H=0}$ at $q=q_{\text{bump}}=10^{-2}$ Å^{-1} is preserved for $S_\perp$, and even slightly enhanced.

(ii) This bump is completely smoothed out for $S_\parallel$ which is almost flat for $q\geqslant3.8\times10^{-2}$ Å^{-1}.

(iii) At small q, the anisotropy of $S(\vec{q})$ is more pronounced. It can be understood as an anisotropy of compress-

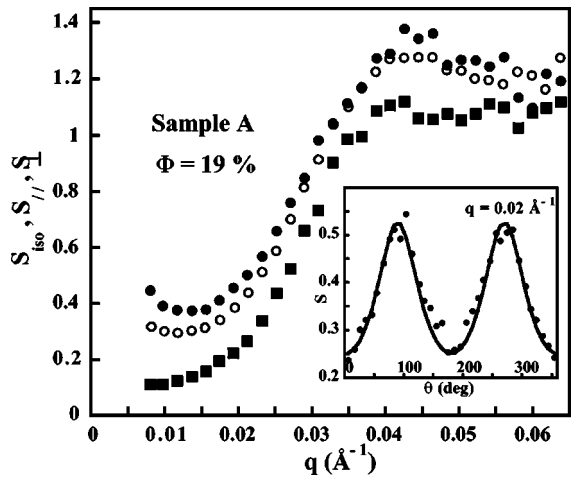

FIG. 10. Sample A at $\Phi=19\%$. Comparison between the q dependencies of the zero field structure factor $S(q,H=0)$ and of the anisotropic one $S(q,H,\theta)$ under $H=68$ kA m^{-1} for $\theta=0$ ($\vec{q}\|\vec{H}$) and $\theta=\pi/2$ ($\vec{q}\perp\vec{H}$). Same symbols as Fig. 9. Inset: Angular dependence of $S(q,H,\theta)$ at $q=2\times10^{-2}$ Å^{-1} and $H=68$ kA m^{-1}.

ibility and of the spatial fluctuations of concentration.

(iv) At small q, the variations of $S(\vec{q})$ as a function of the angle θ at constant q are well fitted by a linear function of $\cos^2(\theta)$ (see the inset of Fig. 10).

2. Anisotropic structure factor coefficients

In a first step we analyze the low q results in a phenomenological way, in terms of an anisotropic coefficient $K_T(H,\theta)$ which controls the global interaction and $b(H,\theta)$ which controls the spatial inhomogeneities of the fluctuations of Φ. Transposing the zero-field expressions (8) and (10) to the under-field situation the structure factor then writes

$$S(q,H,\theta,\Phi)^{-1}=1+K_T(H,\theta)\Phi + (V_w/kT)b(H,\theta)\Phi q^2 \quad \text{at low } \Phi \text{ and } q. \tag{11}$$

Further on, we use the superscripts $\|$ and $\perp$, respectively, for $\theta=0$ and $\theta=\pi/2$. Still for sample A at $\Phi=19\%$, Fig. 11 presents for the two directions the variations of K_T and b with the applied field H. In Fig. 11(a), $K_T^{\|}$ increases with the field, while $K_T^{\perp}$ decreases. In Fig. 11(b), the variations of b are opposite: $b^{\|}$ decreases with the applied field while $b^{\perp}$ increases. This suggests a proportionality between K_T and $-b$. It can be seen in Fig. 11(c) which plots for sample A at $\Phi=19\%$ the ratio $\sqrt{(-b/kT)(V_w/K_T)}$ as a function of H. It is roughly a constant equal to κ_0^{-1} whatever the direction $\|$ or $\perp$. Figure 12(a) shows that the variations of the ratios $K_T^{\perp}/K_T^{\|}$ and $b^{\perp}/b^{\|}$ for samples A and B roughly superimpose as a function of H (note that these ratios go as low as 0.2 at 68 kA m^{-1}). Experimental data thus support the relation

$$\frac{V_w b(H,\theta)}{kT}=-K_T(H,\theta)\kappa_0^{-2}, \tag{12}$$

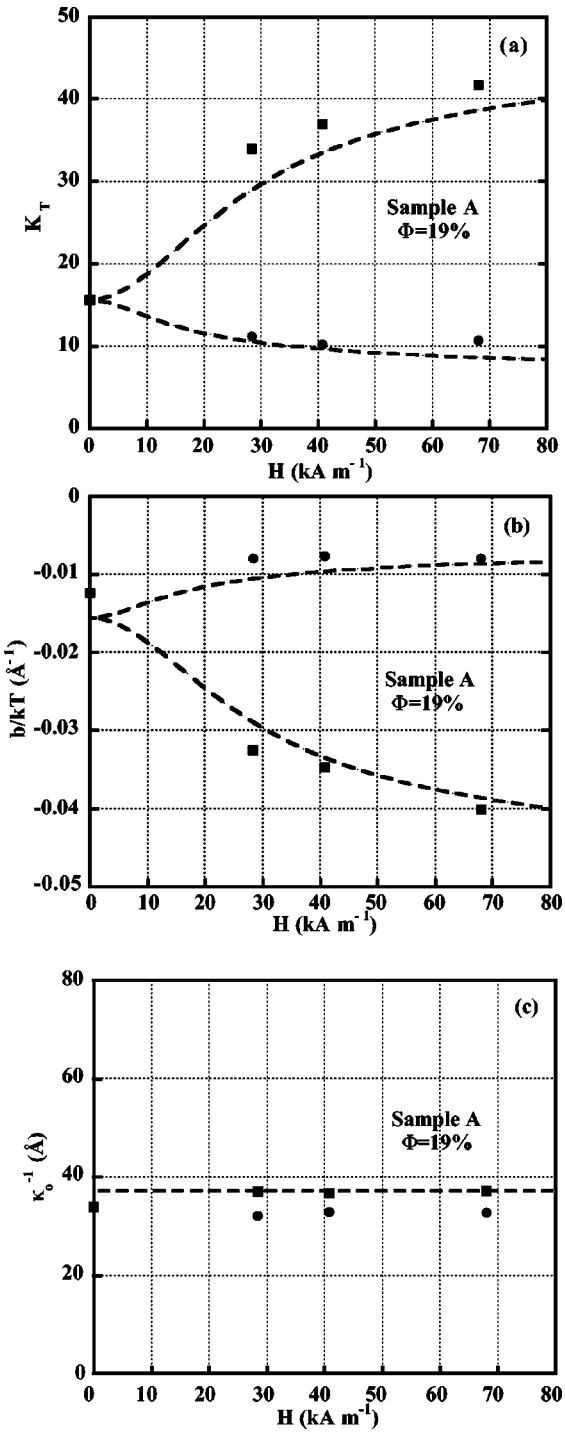

FIG. 11. Sample A at $\Phi=19\%$. Under field anisotropy of the experimental coefficients K_T (a) and b/kT (b). Field independence of the potential range $\kappa_o^{-1}=\sqrt{(-b/kT)(V_w/K_T)}$ (c). Symbols: ■ for $\vec{q}\|\vec{H}$; ● for $\vec{q}\perp\vec{H}$. The dashed lines are deduced from the expressions (11), (12), and (14), α_λ/Φ and β_λ/Φ being calculated from the expressions (B4) and (B11) with $\gamma/\Phi=41$ and $\lambda=0.22$. (The fit gives here $K_T^0=15.6$ and $\kappa_0^{-2}/V_w=10^{-3}$ Å^{-1}.)

where the characteristic length κ_0^{-1} remains independent of H and θ. Note that Eq. (12) reduces to $V_w b_0/kT=-K_T^0\kappa_0^{-2}$ in zero field [Eq. (10)]. It is then possible to rewrite the structure factor as

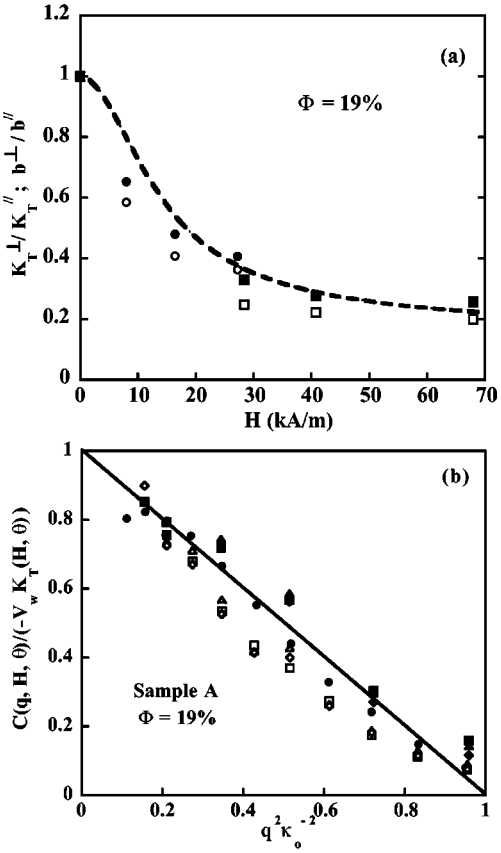

FIG. 12. (a) Comparison of the magnetic field dependence of the ratios $K_T^{\perp}/K_T^{\parallel}$ (full symbols) and $b_{\perp}/b_{\parallel}$ (open symbols) for samples A (■, □) and B (●, ○) at $\Phi=19\%$. The dashed line is deduced from the expressions (11), (12), and (14) (as in Fig. 11). (b) Sample A at $\Phi=19\%$ under various applied fields. $C(q,H,\theta)/-V_w K_T(H,\theta)=[S^{-1}(q,H,\theta)-1]/\Phi K_T(H,\theta)$ as a function of $q^2\kappa_o^{-2}$ [$H=0$: (●); $H=20.5$ kA m^{-1}, $\theta=0$: (□), $\theta=\pi/2$: (■); $H=41$ kA m^{-1}, $\theta=0$: (△), $\theta=\pi/2$: (▲); $H=68$ kA m^{-1}, $\theta=0$:(◇), $\theta=\pi/2$: (◆)]. The full line corresponds to Eq. (13).

$$S(q,H,\theta,\Phi)^{-1}\cong 1+K_T(H,\theta)\Phi(1-q^2\kappa_0^{-2}) \quad \text{at low } \Phi \text{ and } q. \tag{13}$$

The low q anisotropy of the structure factor reduces to an anisotropy of macroscopic compressibility [or of the interaction parameter $K_T(H,\theta)$] which varies linearly with $\cos^2\theta$ at constant field (see the inset of Fig. 10). The validity of such a development up to $\Phi=19\%$ and $q=\kappa_0$ is also supported by Fig. 12(b), which plots the direct correlation function $C(q,H,\theta,\Phi)$ as a function of $q^2\kappa_0^{-2}$ for both $\theta=0$ and $\theta=\pi/2$: the master curve obtained for θ and H expresses that the development of expression (13) is valid up to $q=\kappa_0$.

C. Theoretical derivation of the structure factor

How should we interpret those observations? Let us note that here the scattering is dominantly nuclear, thus the magnetic moment orientation induced by the magnetic field is not detected. As there is not any macroscopic phase separation here, the principal effect then comes from a modification of the dipole-dipole pair potential at the microscopic level. The resulting anisotropy of the fluctuations under field can be determined from the development of the free energy of the system. The formalism used and presented hereafter is based on the same ground as a model previously developed in Refs. [37,38] to describe the field dependence of the massic diffusion coefficient of FF as measured at very low q in a forced Rayleigh scattering experiment. In this experiment an anisotropy of the diffusion coefficient D is observed under field. As on thermodynamic bases, D is inversely proportional to the structure factor of the solution at $q=0$ (and also to the friction coefficient), the anisotropy of D and that of $S(q=0)$ are naturally linked [55].

Our theoretical derivation consists of the small q expansion of the free energy [expression (7)] in the framework of our model [37,38]. As derived in Appendix B the effect of the magnetic field on the interaction parameter $K_T(H,\theta)$ of expression (13) can be written as

$$K_T(H,\theta)=K_T^0-\left[\frac{\alpha_\lambda}{\Phi}\right]_{(i)}+\left[\frac{\beta_\lambda\cos^2\theta}{\Phi}\right]_{(ii)}. \tag{14}$$

This expression contains three terms. The zero-field one, K_T^0, is isotropic and includes all the interactions nondependent on H. There are two contributions coming from the magnetic dipolar interaction under field, and thus dependent on H: (i) A mean field contribution—*isotropic and* basically *attractive*—related to the *mean local fields effects*. It accounts for the short-range aspects of the magnetic dipolar interaction. (ii) An *anisotropic and repulsive* contribution related to the *anisotropic fluctuations of the macroscopic field*. This demagnetizing effect, which increases the energy of the system, accounts for the long-range aspects of the magnetic dipolar interaction.

The details of the calculations of $-\alpha_\lambda/\Phi$ and $\beta_\lambda\cos^2\theta/\Phi$ are given in Appendix B. Let us point out the following.

(i) The two contributions $-\alpha_\lambda/\Phi$ and $\beta_\lambda\cos^2\theta/\Phi$ can be expressed as a function of the effective field parameter λ [see Eq. (3); here taken equal to 0.22 like in [37,38]] as well as of γ and ξ_e [thus ξ through Eq. (3)].

(ii) They saturate in high fields, $-\alpha_\lambda/\Phi$ tends toward $-\lambda_\gamma/\Phi$ (here ≈ 9) and β_λ/Φ tends toward γ/Φ (here ≈ 41).

(iii) The absolute value of $-\alpha_\lambda/\Phi$ is always smaller here than $K_T^0/2$. Thus $K_T(H,\theta)$ *cannot become negative* (even for $\theta=\pi/2$) and the dipole-dipole interaction is not able to destabilize the present colloid *or to induce its particle aggregation*.

D. Comparison between theory and experiment

Figure 11(a) appears thus as an experimental plot of

$$K_T^{\parallel}=K_T^0-\frac{\alpha_\lambda}{\Phi}+\frac{\beta_\lambda}{\Phi} \quad \text{for } \vec{q}\parallel\vec{h}, \tag{15}$$

$$K_T^{\perp}=K_T^0-\frac{\alpha_\lambda}{\Phi} \quad \text{for } \vec{q}\perp\vec{h}$$

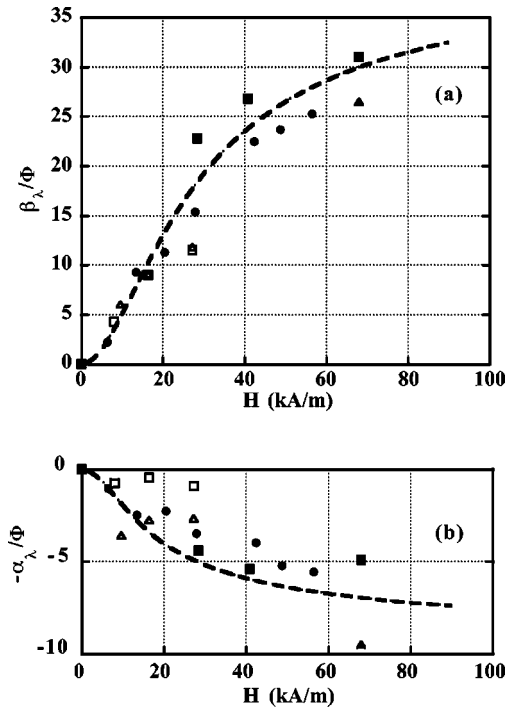

FIG. 13. Field dependence of the coefficients β_λ/Φ (a) and $-\alpha_\lambda/\Phi$, (b) as deduced from the SANS data and expressions (16) and (17)—sample A at $\Phi=19\%$ (■), at $\Phi=6.4\%$ (▲) and sample B at $\Phi=19\%$ (□), at $\Phi=5\%$ (△); from the forced Rayleigh scattering experiment of Refs. [37,38] performed with a FF based on maghemite particles (●); and from theoretical expressions (B4) and (B11) with $\gamma/\Phi=41$ and $\lambda=0.22$ (dashed line).

as a function of the applied field. The field dependence of $-\alpha_\lambda/\Phi$ and β_λ/Φ can then be either calculated from the characteristics of the colloids (see Appendix B) in order to fit the data in Figs. 11(a), 11(b), and 12(a), using expressions (B4) and (B11) from Appendix B [and expression (12) to deduce $b^{\|}/kT$ and $b^{\perp}/kT$ as a function of α_λ/Φ and β_λ/Φ] or deduced from the experimental field dependence of $K_T^{\perp}$ and $K_T^{\|}$ since we know from Eq. (15) that

$$\frac{\beta_\lambda}{\Phi}=K_T^{\|}-K_T^{\perp} \tag{16}$$

and

$$\frac{\alpha_\lambda}{\Phi}=K_T^{\perp}-K_T^{0}. \tag{17}$$

As α_λ/Φ and β_λ/Φ are functions that are weakly dependent on Φ, we can present in the same Figs. 13(a) and 13(b) the theoretical variations of α_λ/Φ and β_λ/Φ deduced from Appendix B and the experimental data using expressions (16) and (17). They are also compared to the previous measurements of α_λ/Φ and β_λ/Φ obtained in the Rayleigh forced experiment [37,38] with a sample of similar dipolar characteristics $\gamma/\Phi=41$. The agreement between the data and the model is reasonable. Note that although α_λ/Φ and β_λ/Φ are expected to saturate in high fields, respectively, to $\lambda(\gamma/\Phi)\approx 9$ and to $\gamma/\Phi\approx 41$ (see Appendix B), this saturation is not fully reached here experimentally for an applied field $H=68\ \mathrm{kA\,m^{-1}}$.

In conclusion, in a monophasic FF under magnetic field, there are fluctuations of macroscopic fields, which are different in the directions parallel and normal to the applied field. The diffusion becomes anisotropic as it introduces a supplementary dispersive force centered along the field and varying linearly with $\cos^2\theta$. This anisotropic dispersive force $[\propto(\beta_\lambda/\Phi)\cos^2\theta]$ is coming from the long-range effect of the dipolar magnetic interaction (the demagnetizing effect). It is here much stronger than the (short-range) mean-field averaged dipolar interaction $(\propto-\alpha_\lambda/\Phi)$. The combination of those two contributions results in an anisotropy of the Brownian motion of the nanoparticles under field and correctly describes the anisotropy of structure factor under field.

V. DISCUSSION

It is common sense to expect that the SANS observation of FF under field would give anisotropic scattering. However, we would like to stress the many unexpected aspects of it.

(1) The most usual signal in a magnetic system under field (e.g., ferromagnetic steel) is ''eightlike'' patterns oriented perpendicular to the field [35,56]. The reason is that magnetic scattering is null when q is parallel to the field. Here we observe rather similar patterns, but the magnetic scattering is negligible. We have only nuclear scattering, revealing the positions of the particles.

(2) If we focus on spatial positions, we could meet a second well-known expectation, following de Gennes and Pincus, namely chaining of particles along the field. In principle, *such chaining should produce* at the scale of the diameter of particles a pronounced maximum of the structure factor $[S_{\|}(q)]$ in the direction parallel to H, corresponding to the first neighbors along the chain as predicted in [34]. *However, in our system we observe just the opposite*: both the maximum and the zero q limit are stronger in the perpendicular direction. This is correctly accounted for by our proposed derivation of the scattering, and therefore explained.

(3) Though our model gives a good description of the patterns observed here in this paper, we want to stress the fact that it can give *quite different degree of anisotropy* depending on the system under study. At $q=0$, the maximum anisotropy of the pattern can be, for example, quantified by the ratio

$$\frac{K_T^{\|}-K_T^{\perp}}{K_T^{\perp}}=\frac{\dfrac{\beta_\lambda}{\Phi}}{K_T^{0}-\dfrac{\alpha_\lambda}{\Phi}}, \tag{18}$$

which reaches here a value of the order of 4.3. Yet, experimentally, the SANS pattern of a ferrofluid under magnetic field is not always anisotropic [42,43]. In particular, the sample A of Ref. [22] ($d_o=7.1$ nm; $\sigma=0.15$; $d_w=8.3$ nm) does not present any anisotropy under a field of 68 kA/m at $\Phi=11\%$. This point can be explained by a very different

situation: in this colloid repulsion is very strong, such that $K_T^0 \cong 33$ with $\gamma/\Phi = 11$, which leads to a ratio $(\beta_\lambda/\Phi)/[K_T^0 - (\alpha_\lambda/\Phi)]$ of the order of 5%. The field effect is then 100 times smaller than in the present work.

A. Behavior at various scales

At large spatial scales (low scattering vectors: $q \leqslant \kappa_0$), we extract the following from the experimental data:

(i) A length κ_0^{-1} characteristic of the range of the pair potential which does not present any significant anisotropy under field, up to $\Phi \cong 19\%$.

(ii) A strongly anisotropic compressibility felt under field at a long spatial range.

(iii) An always positive interaction parameter $K_T(H,\theta)$ whatever H and θ. Increasing even more the magnetic field would not modify this point as α_λ/Φ would saturate here at a value $\lambda(\gamma/\Phi) \cong 9$ still smaller than K_T^0.

(iv) An always negative b_0 coefficient associated with the contribution of the spatial inhomogeneities of concentration to the free energy. The fluctuations of position of individual particles are associated with a correlation hole. Under field those individual fluctuations of position are anisotropic.

If our model satisfactorily explains large spatial scale behaviors, a precise description of the detailed local structure of the ferrofluid under field is yet to be done. We have, however, several indicators for this description from the structure factor at $q \geqslant \kappa_0$:

(i) The peak at high Φ, which is more pronounced in $I_\parallel(q)$ than in $I_\perp(q)$ under field, while it is the opposite for $S(q)$, for which the maximum vanishes for $S_\parallel(q)$. In that direction the field seems to unstructure the fluid system, which looks like a ''gas'' in that direction with no local structure (the structure factor is flat at high q).

(vi) The peak abscissa, which does not appear significantly modified with respect to its value in zero field, in the direction normal to the applied field; in as much as it represents an interparticle distance (in the direct space), the latter does not seem to vary. However a serious account of the meaning of the peak, in particular with respect to the particle size, would be easier with much less polydisperse samples.

B. Handwaving picture

All this can be summarized in a handwaving explanation. *Along the field*, because of the demagnetizing effect, spatial inhomogeneities of magnetic field are expensive in energy: the system prefers to lower them, hence to lower the concentration fluctuations as much as possible (increasing the fluctuations of position of the nanoparticles). Meanwhile *in the transverse direction*, these demagnetizing field effects vanish [$\theta = 0$ in Eq. (14)]. However, in the transverse direction we only observe the other—isotropic—effect of the field: the fluctuations of concentration are slightly larger than under zero field because of the short range isotropic and attractive contribution of the (mean-field averaged) interaction between magnetic dipoles, which slightly decreases the fluctuations of position of the nanoparticles.

Those anisotropic local fluctuations of nanoparticle positions smooth down the maximum of $S(q)$ in the direction parallel to the field. It is those local fluctuations that render the system macroscopically less compressible in the direction parallel to the field than in the normal one. In real space, the system looks like a gas in the direction parallel to the field, while it keeps its fluid structure perpendicularly to the field.

We have seen that there is no real chaining, since the particles are not coming in static close contact to each other to produce compact elongated chains. This would be detected by the observation of a clear maximum of $S_\parallel(q)$ in the contact condition. However, the strong difference in fluctuations of concentration (and of nanoparticle positions) along and perpendicular to the field can be phrased as creating a kind of *interaction chaining* via the structuration perpendicular to the field.

VI. SUMMARY AND PERSPECTIVES

We have studied experimentally the nuclear part of the SANS pattern, here only related to particle positions, of an ionic magnetic colloid far from the conditions of colloidal destabilization.

In zero field the SANS pattern is isotropic. A fluidlike structure is found for the colloid: with large enough volume fractions, a maximum of the structure factor is observed for the mean interparticle distance. From a standard Landau-Ginzburg free energy, we derive the structure factor at small scattering vectors (large distances). Besides the particle size characteristics V_w and R_g, two quantities characterizing the pair interparticle potential are measured at low q: the interaction parameter K_T^0 (proportional to the second virial coefficient), which is found positive, meaning that the potential is globally repulsive, and its range κ_0^{-1} of the order of 30 Å at $\Phi = 19\%$. The coefficient b_0 associated in the model to the spatial inhomogeneities of concentration fluctuations $[-\frac{1}{2} b_0 (\nabla \delta\Phi)^2$ in the free energy] is always negative here, being equal to $-(kT/V_w) K_T^0 \kappa_0^{-2}$.

Under field the SANS pattern is anisotropic. This anisotropy is coming from the structure factor of the solution and can be analyzed at different scales.

At low q the effective compressibility of the system is found anisotropic: while the characteristic length κ_0^{-1} remains isotropic under field, the interaction parameter K_T and the coefficient b are both strongly anisotropic. A quantitative analysis shows that these low q anisotropies are here due to the long range magnetic interaction. The interaction of the medium with the magnetic field is introduced through two contributions added to the zero-field description. The first one, isotropic, modelizes the local field effects. It corresponds to an increased attraction of the pair potential when magnetic moments are aligned along the field. The second one, anisotropic, modelizes the long range demagnetizing field effect, associated with the fluctuations of magnetization. It reduces any strong concentration fluctuations along the field because they would provoke strong field gradients.

At q larger than κ_0, we observe a smoothing of the structure factor in the direction parallel to the field while the fluidlike zero-field structure is roughly preserved in the per-

pendicular directions. In the direction parallel to the field the system appears like a gas.

All these results lead to the following interpretation—the fluctuations of concentration in the system are smoothed along the field—they are associated with fluctuations of position of the particles, which are increased along the field and decreased in the perpendicular directions. This means that the local Brownian motion of the nanoparticles is anisotropic here. It also explains why we do not observe under field any close-contact chaining of the nanoparticles. On the contrary, we could describe the observed uniaxial anisotropic structure as that of a pseudo-one-dimensional gas along the field coupled to a more compressible fluidlike structure in the two perpendicular directions. We propose to call ''interaction chaining,'' such a uniaxial structure coming from the transverse fluidlike structuration.

As a future development of this work, we shall study how the diffraction pattern would be modified under rotation in order to analyze the local competition of the dipolar interaction under field with the vorticity of the solid rotation. We shall then connect the direct observation of the local structure of the FF to magneto-rheological measurements as obtained in [19,20].

Another interesting question to elucidate would be what happens if the colloid is in a less repulsive situation if it is closer to the colloidal phase separation in zero field and thus has a reduced interaction parameter K_T^0 ? It is then possible to imagine a hybrid situation with $K_T^{\perp}<0$ and $K_T^{\parallel}>0$; that is a system potentially unstable in the direction perpendicular to the field remaining stable in the field direction. Note that some experimental observations come to support such a possibility: concentrated phase droplets (in a phase separated sample close to the threshold) observed by optical microscopy exhibit a strong anisotropy of surface tension, as is predicted by recent numerical simulations [57].

ACKNOWLEDGMENTS

We thank Sophie Neveu for the chemical synthesis of the ferrofluid samples, Annie Brulet for her help in the polarization analysis of the neutron scattering, Fabrice Cousin for showing us his not-yet-published results, and Pierre Levitz for helpful discussions.

APPENDIX A

Let us first come back to the development of $S(q,\Phi)$ written in Eq. (10). This development has to be distinguished from the more classical following development [58]:

$$\frac{1}{S(q,\Phi)}=\frac{V_w b_0}{kT}\Phi\xi_c^{-2}(1+q^2\xi_c^2), \tag{A1}$$

which is meaningful near a second order phase transition threshold. In Eq. (A1), ξ_c corresponds to the characteristic length of the fluctuations of concentration, and diverges at the critical point. The link between the two lengths κ_0^{-1} and ξ_c, respectively, defined in Eqs. (10) and (A1) is

$$\xi_c^{-2}=-K_T^0\kappa_0^{-2}\frac{\Phi}{1+K_T^0\Phi}=\frac{V_w b_0}{kT}\frac{\Phi}{1+K_T^0\Phi}. \tag{A2}$$

As the quantity $1+K_T^0\Phi=\lim_{q\to 0}(1/S)$ is always positive, ξ_c^2 is of the same sign as b_0. We recall that this coefficient b_0 is defined in Eq. (7) and related to K_T^0 and κ_0^{-1} by Eq. (10),

$$b_0=-\frac{kT}{V_w}K_T^0\kappa_0^{-2}.$$

Two main opposite situations can be encountered: (i) If the interparticle potential is globally attractive then $K_T^0<0$, $\kappa_0^{-2}>0$, $b_0>0$, and $\xi_c^2>0$. In that case the system presents concentration fluctuations with a characteristic correlation length ξ_c. It tends to phase separate, see for example [44,58,59]. (ii) If the interparticle potential is globally repulsive then $K_T^0>0$, $\kappa_0^{-2}>0$, $b_0<0$, and $\xi_c^2<0$. The length ξ_c is not defined. There is no correlation domain for the fluctuations of concentration. The individual fluctuations of position of the particles are associated with a correlation hole of order κ_0^{-1}, the spatial range of the pair potential (repulsive on average). The system remains monophasic. It is the situation of the present work.

Note that experimentally, some intermediate situations may be observed if K_T^0 and b_0 are small: they do not come to zero exactly together. Then Eq. (7) has to be developed at a higher order in $\delta\Phi$.

APPENDIX B

In the framework of our model, the effect of the magnetic field on the compressibility of the system is separated into two contributions.

(i) *An isotropic mean-field one*, related to the *mean* local field, which modifies the zero field interaction parameter K_T^0 entering in expression (7) [via Eqs. (9) and (10)]. On average, the dipolar interaction is globally attractive. It modifies the zero-field chemical potential φ_0 and transforms it in $\varphi=\varphi_0+\varphi_H$. The additional term φ_H has to take into account the effect of the applied field and that of the local field induced by the whole magnetic solution. In an effective field model [see expressions (2) and (3)] it writes [3,37]

$$\varphi_H=-kT\ln\left(\frac{\sinh(\xi_e)}{\xi_e}\right), \tag{B1}$$

where the effective Langevin parameter ξ_e depends on the effective field constant λ and on the dipolar interaction parameter γ [Eq. (4)]. As

$$K_T^0=\frac{1}{\Phi}\left(\frac{1}{kT}\frac{\partial\pi}{\partial\Phi}-\frac{1}{V_w}\right)=\frac{1}{kT}\frac{\partial\varphi_0}{\partial\Phi}-\frac{1}{\Phi} \tag{B2}$$

the interaction parameter then rewrites under field

$$K_T=\frac{1}{kT}\frac{\partial\varphi}{\partial\Phi}-\frac{1}{\Phi}\quad\text{with}\frac{\partial\varphi}{\partial\Phi}=\frac{\partial\varphi_0}{\partial\Phi}+\frac{\partial\varphi_H}{\partial\Phi}. \tag{B3}$$

Taking into account that

$$\frac{\partial \varphi_0}{\partial \Phi} = \frac{kT}{\Phi}(1 + K_T^0 \Phi)$$

and from Eq. (B1) that

$$\frac{\partial \varphi_H}{\partial \Phi} = -kTL(\xi_e)\frac{\partial \xi_e}{\partial \Phi} = -\frac{kT}{\Phi}\frac{\lambda \gamma L^2(\xi_e)}{1-\lambda \gamma L'(\xi_e)},$$

it comes to

$$K_T = K_T^0 - \frac{\alpha_\lambda}{\Phi} \quad \text{with} \quad \alpha_\lambda = \lambda \gamma \frac{L^2(\xi_e)}{[1-\lambda \gamma L'(\xi_e)]}, \quad \text{(B4)}$$

keeping the same notation α_λ as in [37,38]. The reduction α_λ/Φ of the interaction coefficient is null in zero field and saturates at $\lambda\gamma/\Phi$ in high fields where all the magnetic moments are aligned along the field. Taking, as in [37,38], $\lambda = 0.22$ for a rough evaluation, α_λ/Φ is always smaller here than $K_T^0/2$. Thus here, K_T *cannot become negative* (for our samples and whatever the magnetic field would be).

(ii) *An anisotropic contribution* related to the *fluctuations of macroscopic field*. It leads to a supplementary magnetic term in the expression (7) of the free energy

$$\frac{\mu_0}{2}\mu_{NL}(\delta \vec{H})^2, \quad \text{(B5)}$$

$\mu_{NL} = 1 + \partial M/\partial H$ being the differential permeability (here assumed isotropic). In the framework of the linear response $\vec{M} = \chi_0 \vec{H}$, μ_{NL} would reduce to $1+\chi_0$.

This demagnetizing term exists only under applied field $\vec{H}$. It is due to the local inhomogeneities of magnetization in the medium. It grounds in the continuity conditions of $\vec{H}$ at the boundaries between the regions with different concentrations of magnetic nanoparticles. They introduce anisotropic gradients of macroscopic field, which lead to anisotropic fluctuations of concentration and anisotropic diffusion.

$\partial M/\partial H$ is obtained in the framework of the effective field model from Eqs. (2) and (3),

$$\mu_{NL} = \frac{1+\gamma(1-\lambda)L'(\xi_e)}{1-\lambda\gamma L'(\xi_e)}. \quad \text{(B6)}$$

The magnetic field strength $\delta\vec{H}$ in the perturbed state is obtained from the continuity equation of the perturbed magnetic induction,

$$\mu_{NL}\,\mathrm{div}(\delta \vec{H}) = -\mathrm{div}\left(\frac{\partial \vec{M}}{\partial \Phi}\delta\Phi\right). \quad \text{(B7)}$$

It comes by Fourier transformation, $\vec{M}$ and $\vec{H}$ being colinear to the unit vector $\vec{h}$,

$$\delta \vec{H}_{\vec{q}} = -\frac{1}{\mu_{NL}}\frac{\partial M}{\partial \Phi}\frac{\vec{q}(\vec{q}\vec{h})}{q^2}\delta\Phi_{\vec{q}}, \quad \text{(B8)}$$

where $\partial M/\partial\Phi = m_S L(\xi_e)/[1-\lambda\gamma L'(\xi_e)]$ as deduced from Eqs. (2) and (3).

Thus the supplementary magnetic term $(\mu_0/2)\mu_{NL}(\delta\vec{H})^2$ in Eq. (7) of the free energy changes the probability of the fluctuations of concentration. The mean value of the volume fraction fluctuations becomes

$$\langle |\delta\Phi_{\vec{q}}|^2 \rangle = \frac{kT\Phi}{\frac{\partial \pi}{\partial \Phi} + b\Phi q^2 + \frac{\mu_0 \Phi}{\mu_{NL}}\left(\frac{\partial M}{\partial \Phi}\right)^2 \cos^2\theta} \quad \text{(B9)}$$

with $(\vec{q}\vec{h})^2/q^2 = \cos^2\theta$. It leads [37,38] to a new term in the development, at the first order in q and Φ, of the structure factor $S(q,H,\theta,\Phi)$ [expressions (8) and (10)] which now is written as

$$S(q,H,\theta,\Phi)^{-1} = 1 + K_T^0\Phi - \alpha_\lambda + \beta_\lambda \cos^2\theta - \frac{V_w b}{kT}\Phi q^2 \quad \text{(B10)}$$

with

$$\beta_\lambda = \frac{V_w}{kT}\frac{\mu_0\Phi}{\mu_{NL}}\left(\frac{\partial M}{\partial \Phi}\right)^2 = \frac{\gamma L^2(\xi_e)}{[1-\lambda\gamma L'(\xi_e)][1+(1-\lambda)\gamma L'(\xi_e)]}. \quad \text{(B11)}$$

This term $\beta_\lambda \cos^2\theta$ expresses the existence of anisotropic fluctuations in the now anisotropic medium. It is proportional to $\cos^2\theta$ and produces the anisotropy of $S(\vec{q})$. Null if $\vec{q}\perp\vec{h}$, this term is maximum for $\vec{q}\parallel\vec{h}$. The gain $\beta_\lambda \cos^2\theta/\Phi$ of the interaction coefficient is null in zero field and saturates at $\gamma\cos^2\theta/\Phi$ in high fields where all the magnetic moments are aligned along the field.

Combining the two contributions (i) and (ii), the anisotropic interaction parameter $K_T(H,\theta)$ of expression (13) writes as

$$K_T(H,\theta) = K_T^0 - \frac{\alpha_\lambda}{\Phi} + \frac{\beta_\lambda \cos^2\theta}{\Phi}. \quad \text{(B12)}$$

It is also expression (14). This macroscopic term, calculated in the thermodynamic limit, is only relevant in the limit of small q vectors.

[1] R. Rosensweig, *Ferrohydrodynamics* (Cambridge University Press, Cambridge, 1985).
[2] M. I. Shliomis, Sov. Phys. JETP **34**, 1291 (1972).
[3] E. Blums, A. Cebers, and M. M. Maiorov, *Magnetic Fluids* (de Gruyter, New York, 1997).
[4] P. G. de Gennes and P. Pincus, Phys. Kondens. Mater. **11**, 189 (1970).
[5] M. Widom and H. Zhang, in *Complex Fluids*, edited by E. Sirpta, D. Weitz, T. Witten, and J. Israelachvili, Mater. Res. Soc. Symp. Proc. No. 248 (Materials Research Society, Pittsburgh, 1992), p. 235.
[6] R. W. Chantrell, A. Bradbury, J. Popplewell, and S. W. Charles, J. Appl. Phys. **53**, 2742 (1982).
[7] B. E. Kashevsky, J. Magn. Magn. Mater. **122**, 34 (1993).
[8] M. E. van Leeuwen and B. Smit, Phys. Rev. E **51**, 5976 (1995).
[9] M. J. Stevens and G. S. Grest, Phys. Rev. Lett. **72**, 3686 (1994).
[10] G. Helgesen, A. T. Skjeltorp, P. M. Mors, R. Botet, and R. Jullien, Phys. Rev. Lett. **61**, 1736 (1988).
[11] T. Tlusty and S. A. Safran, Science **290**, 1328 (2000).
[12] Y. Graselli, G. Bossis, and E. Lemaire, J. Phys. II **4**, 253 (1994).
[13] F. Leal-Calderon, T. Stora, O. Mondain-Monval, P. Poulin, and J. Bibette, Phys. Rev. Lett. **72**, 2959 (1994).
[14] E. M. Lawrence, M. L. Ivey, G. A. Flores, J. Liu, J. Bibette, and J. Richard, Int. J. Mod. Phys. B **8**, 2765 (1994).
[15] J. H. Promislow and A. P. Gast, Langmuir **12**, 4095 (1996).
[16] E. M. Furst and A. P. Gast, Phys. Rev. E **58**, 3372 (1998).
[17] S. Cutillas, G. Bossis, E. Lemaire, A. Meunier, and A. Cebers, Int. J. Mod. Phys. B **13**, 1791 (1999).
[18] G. A. Flores, Jing-Liu, M. Mohebi, and M. Jamasbi, Phys. Rev. E **59**, 751 (1999).
[19] F. Gazeau, C. Baravian, J.-C. Bacri, R. Perzynski, and M. I. Shliomis, Phys. Rev. E **56**, 614 (1997).
[20] F. Gazeau, B. M. Heegaard, J.-C. Bacri, A. Cebers, and R. Perzynski, Europhys. Lett. **35**, 609 (1996).
[21] E. Dubois, V. Cabuil, F. Boué, J. C. Bacri, and R. Perzynski, Prog. Colloid Polym. Sci. **104**, 173 (1997).
[22] E. Dubois, V. Cabuil, F. Boué, and R. Perzynski, J. Chem. Phys. **111**, 7147 (1999).
[23] E. Dubois, R. Perzynski, F. Boué, and V. Cabuil, Langmuir **16**, 5617 (2000).
[24] H. Zhang and M. Widom, Phys. Rev. E **49**, R3591 (1994).
[25] V. Russier, J. Colloid Interface Sci. **174**, 166 (1995).
[26] R. P. Sear, Phys. Rev. Lett. **13**, 2310 (1996).
[27] D. Lacoste and T. C. Lubensky, Phys. Rev. E **64**, 041506 (2001).
[28] R. Anthore, C. Petipas, D. Chandesris, and A. Martinet, J. Phys. (Paris), Colloq. **38**, C2-203 (1977).
[29] R. Anthore, S. Gauthier, A. Martinet, and C. Petipas, IEEE Trans. Magn. **MAG-16**, 197 (1980).
[30] D. J. Cebula, S. W. Charles, and J. Popplewell, J. Phys. (France) **44**, 207 (1983).
[31] R. Rosman, J. J. M. Janssen, and M. Th. Rekveldt, J. Magn. Magn. Mater. **85**, 97 (1990).
[32] J. Lal, D. Abernathy, L. Auvray, O. Diat, and G. Grübel, Eur. Phys. J. E **4**, 263 (2001).
[33] P. Licinio, A. V. Teixeira, G. A. M. Safar, M. S. Andrade, L. C. Meira-Belo, and U. A. Leitao, J. Magn. Magn. Mater. **226-230**, 1986 (2001).
[34] J. B. Hayter and R. Pynn, Phys. Rev. Lett. **49**, 1103 (1982).
[35] R. Pynn, J. B. Hayter, and S. W. Charles, Phys. Rev. Lett. **51**, 710 (1983).
[36] F. Gazeau, E. Dubois, F. Boué, S. Neveu, and R. Perzynski (unpublished).
[37] J.-C. Bacri, A. Cebers, A. Bourdon, G. Demouchy, B. M. Heegaard, and R. Perzynski, Phys. Rev. Lett. **74**, 5032 (1995).
[38] J.-C. Bacri, A. Cebers, A. Bourdon, G. Demouchy, B. M. Heegaard, B. Kashevsky, and R. Perzynski, Phys. Rev. E **52**, 3936 (1995).
[39] R. Massart, E. Dubois, V. Cabuil, E. Hasmonay, and R. Perzynski, J. Magn. Magn. Mater. **149**, 1 (1995).
[40] J. L. Dormann, D'Orazio, F. Lucari, E. Tronc, P. Prené, J. P. Jolivet, D. Fiorani, R. Cherkaoui, and M. Nogues, Phys. Rev. B **53**, 14291 (1996).
[41] F. Gazeau, E. Dubois, M. Hennion, R. Perzynski, and Yu. Raikher, Europhys. Lett. **40**, 575 (1997).
[42] E. Dubois, thèse, Université Paris 6, France, 1997.
[43] F. Cousin, thèse, Université Paris 6, France, 2000.
[44] F. Cousin, E. Dubois, and V. Cabuil, J. Chem. Phys. **115**, 6051 (2001).
[45] R. E. Rosensweig and J. Popplewell, *Elsevier Studies in Applied Electromagnetics in Materials* (Elsevier, Amsterdam, 1992), Vol. 1, p. 83.
[46] V. Cabuil, R. Perzynski, and J. Bastide, Prog. Colloid Polym. Sci. **97**, 75 (1994).
[47] S. Neveu-Prin, F. A. Tourinho, J.-C. Bacri, and R. Perzynski, Colloids Surf., A **80**, 1 (1993).
[48] *Magnetic Fluids and Applications Handbook*, edited by B. Berkovsky (Begell House, New York, 1996).
[49] C. Kittel, *Introduction to Solid State Physics* (Wiley, New York, 1967), p. 373.
[50] C. Bellouard, I. Mirebeau, and M. Hennion, Phys. Rev. B **53**, 5570 (1996).
[51] L. D. Landau and E. M. Lifshitz, *Statistical Physics* (Pergamon Press, London, 1959), p. 367.
[52] J. W. Cahn and J. E. Hilliard, J. Chem. Phys. **28**, 258 (1958).
[53] J. P. Hansen and I. R. Mac Donald, *Theory of Simple Liquids* (Academic, London, 1990), pp. 172 and 364.
[54] J.-C. Bacri, F. Boué, V. Cabuil, and R. Perzynski, Colloids Surf., A **80**, 11 (1993).
[55] A. Katchalsky, Z. Alexandrowicz, and O. Kedem, *Chemical Physics of Ionic Solutions*, edited by B.E. Connery and R.G. Barradas (Wiley, New York, 1966).
[56] G. E. Bacon, *Neutron Diffraction* (Oxford University Press, Oxford, 1962), p. 173.
[57] A. Cebers, J. Magn. Magn. Mater. (to be published).
[58] P. M. Chaikin and T. C. Lubensky, *Principles of Condensed Matter Physics* (Cambridge University Press, New York, 1995).
[59] D. Stauffer and A. Aharony, *Introduction to Percolation Theory*, revised 2nd ed. (Taylor and Francis, London, 1994).